Deep-learning feature extraction with their subsequent selection and support vector machine classification of the breast ultrasound images

A.A. Kolchev [1], D.V. Pasynkov [2,3], I.A. Egoshin [2], I.V. Kliouchkin [4], O.O. Pasynkova [2]
[1] Kazan (Volga region) Federal University, Ministry of Education and Science of Russian Federation, 420008, Kazan, Russia, Kremlevskaya St. 18;
[2] Mari State University, Ministry of Education and Science of Russian Federation, 424000, Yoshkar-Ola, Russia, Lenin square 1;
[3] Kazan State Medical Academy - Branch Campus of the Federal State Budgetary Educational Institution of Further Professional Education «Russian Medical Academy of Continuous Professional Education», Ministry of Healthcare of the Russian Federation, 420012, Kazan, Russia, Butlerova St 36;
[4] Kazan Medical University, Ministry of Health of Russian Federation, 420012, Kazan, Russia, Butlerova St. 49

Abstract

Our study aimed to develop a comprehensive system for discriminating between benign and malignant breast lesions on ultrasound images. The system integrated deep learning (DL) and conventional machine learning techniques. Our database consisted of 494 ultrasound images, comprising 231 benign and 263 malignant breast lesions. In the initial stage, we evaluated the performance of non-modified DL networks, including VGG-16, ResNet-18, and InceptionRes-NetV2. We assessed the results for the entire lesion as well as its inner and outer parts. For training the networks, we employed supervised transfer learning. In the second stage, we utilized a support vector machine (SVM) model for lesion classification. The features obtained from the modified DL networks, where we removed the last layers, were used for training and testing the SVM. In the final stage, we assessed the classification results using SVM, with a focus on selecting the most significant features obtained from the modified DL networks. We employed techniques such as ReliefF, FSCNCA, and LASSO for feature selection. Our three-step approach yielded impressive results, with an accuracy of 0.987, sensitivity of 0.989, and specificity of 0.983. These results significantly outperformed using only DL or DL + SVM without feature selection. Overall, our algorithm demonstrated sufficient accuracy in the clinical task of discriminating between benign and malignant breast lesions on ultrasound images.

Keywords: ultrasound image, lesion, deep learning, SVM, feature extraction.

Citation: Kolchev AA, Pasynkov DV, Egoshin IA, Kliouchkin IV, Pasynkova OO. Deep-learning feature extraction with their subsequent selection and support vector machine classification of the breast ultrasound images. Computer Optics 2024; 48(5): 753-761. DOI: 10.18287/2412-6179-CO-1421.

Acknowledgements: The main results of sections "Materials and methods" and "Results" were obtained by D.V. Pasynkov and I.A. Egoshin with the support by Grant of Russian Science Foundation (Project 22-71-10070, https://rscf.ru/en/project/22-71-10070/). The authors are grateful to the Kazan Federal University Strategic Academic Leadership Program (PRIORITY-2030) for the technical feasibility of using hardware and software.

Introduction

Breast cancer is a significant global health issue, with a high number of new cases and mortality rates. In 2020, breast cancer became the most prevalent cancer globally, accounting for 11.7 % of all new cases (2,261,419) and surpassing lung cancer (2,206,771 new cases). It is the fifth leading cause of cancer-related deaths worldwide, with 685,000 lethal cases. In women BC is the leading malignancy in the majority (159 of 185) of countries that responsible for the 47.8 % of the new cases among all the cancers. Moreover, BC holds the first rank for malignancy-related mortality in 110 countries [1].

The one of the established strategy to decrease the BC-related mortality is the population-wide mammography screening. It was demonstrated that the regular (every 1 – 2 years) invitation for mammography reduced the BC-related mortality in women 50 – 69 years old (among them only 60 % actuary performed mammography regularly) by 25 % (relative risk (RR): 0.75; 95 % confidence interval [CI]: 0.69–0.81). At the same time in women of this subgroup who actually performed the regular mammography the reduction of the BC-related mortality reached 38 % (RR: 0.62; 95 % CI: 0.56 – 0.69) [2]. However in women of 40 – 44 и 45 – 49 years old the results were less promising. International Agency for Research on Cancer (IARC) Handbook Working Group assessed the strength of evidence that mammography screening decreases the BC-related mortality as limited, and the RR values were not calculated [3]. The reduced effectiveness

of mammography screening in younger women is attributed to the higher proportion of dense breast tissue in this age group. Dense breast tissue can lower the sensitivity of mammography, resulting in reduced detection rates ranging from 50.0 % to 68.1 % compared to 85.7 % to 88.8 % in fatty breast [4].

The supplementation of ultrasound to mammography has been shown to increase the breast cancer detection rate in women with dense breast tissue, from 1.1 to 7.2 cases per 1000 high-risk patients. Notably, 92 % of the breast cancers identified solely through ultrasound were invasive, with a median size of 10 mm, and 89 % of them did not involve metastatic regional lymph nodes [5]. However, the use of ultrasound is also associated with additional non-necessary interventions in 4.9 % of cases and surgical biopsies for benign lesions in 0.9 % of cases, leading to increased costs [6]. Consequently, there is a need to enhance the ultrasound specificity in distinguishing between benign and malignant breast lesions.

The aim of our study was to develop an innovative breast ultrasound discrimination system that combines deep learning (DL) algorithms with conventional approaches.

1. Materials and methods

The study utilized ultrasound systems, including Medison SA8000SE, Siemens X150, Esaote MyLab C, and Mindray DX-8 EX, to acquire digitized 8-bit ultrasound images of the breast. The database consisted of 494 ultrasound images, with 231 confirmed benign and 263 confirmed malignant lesions (as indicated by cytology and / or histology). The image dataset exhibited a wide range of lesion visual appearances commonly observed in both benign and malignant breast lesions (tab. 1). Additionally, distinguishing between benign and malignant lesions visually proved challenging in many cases due to their striking similarity (see fig. 1). The data we used contained no personal patient information.

In each breast ultrasound image, a region of interest (ROI) was manually chosen. The contour of the lesion within the selected ROI was automatically determined using the method described earlier [7].

Within the ROI, the internal and external (belt) parts of the lesion were differentiated. Since the ultrasound signal weakens as it penetrates deeper into the tissues, we focused solely on the upper segment of both the internal and external parts of the lesion that faced the ultrasound probe.

The algorithm for extracting the inner and belt parts is depicted in fig. 2. The source image shows the contour of the lesion marked by a tracing line in fig. 2*a*. Inside the selected contour, the gravity center of the pixel brightness (point *C* in fig. 2*b*) was determined. From point *C*, rays were symmetrically drawn vertically (white lines in fig. 2*b*) until they intersected with the contour. The angle between the marginal rays was set to 60 °. Vertical lines were then drawn from the points of intersection between the rays and the contour. The area enclosed by the vertical lines, the horizontal line passing through point *C*, and the contour line corresponds to the inner part of the lesion (fig. 2*b*). The region above the contour constitutes the belt part of the lesion.

Tab. 1. Characteristics of the lesions included into the analysis. Note: percent values are given for columns. Percent sums may not correspond to 100 % due to the rounding

Type	Size				Total
	≤10 mm	11-20 mm	21-50 mm	>50 mm	
Solid lesions (*n* = 369, 74.70 %)					
Fibroadenoma	6 4.92 %	21 11.8 %	16 10.6 %	–	43 8.70 %
Breast carcinoma	53 43.4 %	87 49.1 %	80 52.9 %	35 70.0 %	255 51.6 %
Focal fibrosis	13 10.6 %	13 7.34 %	–	–	26 5.26 %
Cystadenopapilloma	1 0.82 %	1 0.56 %	–	–	2 0.40 %
Metastases	1 0.82 %	3 1.69 %	1 0.66 %	–	5 1.01 %
Lymphoma	–	2 1.12 %	1 0.66 %	–	3 0.61 %
Sclerosing adenosis	3 2.46 %	6 3.39 %	–	–	9 1.8 %
Lipoma	–	10 5.65 %	8 5.30 %	–	18 3.6 %
Inflammatory infiltrate	–	1 0.56 %	1 0.66 %	1 2.00 %	3 0.6 %
Gynecomastia	–	–	2 1.32 %	–	2 0.4 %
Phylloid	–	1 0.56 %	–	–	1 0.20 %
Intramammary lymph node	1 0.82 %	1 0.56 %	–	–	2 0.2 %
Fluid-filled lesions (*n* = 125, 25.30 %)					
Simple cyst	30 24.6 %	20 11.3 %	31 20.5 %	10 20.0 %	91 18.4 %
Complex cyst (including galactocele)	5 4.10 %	5 2.82 %	3 1.99 %	–	13 2.6 %
Seroma	–	3 1.69 %	4 2.65 %	–	7 1.4 %
Abscess	–	–	1 0.66 %	3 6.00 %	4 0.8 %
Hematoma	–	1 0.56 %	3 1.32 %	1 2.00 %	5 1.0 %
Sebaceous cyst	3 2.46 %	2 1.12 %	–	–	5 1.0 %
Total	**122 24.7 %**	**177 35.8 %**	**151 30.5 %**	**50 10.1 %**	**494 100 %**

All three images (the entire image, images of the internal and external lesion parts) were inputted into the deep learning network to extract image features.

The initial models were based on the MATLAB package models trained on the ImageNet database [8]. These models were fine-tuned on our data with modifications made to the final layers, as the original models were designed for 10000 classes while our task required classification for two classes. Deep learning networks such as VGG16, ResNet-18, and InceptionResNetV2 were considered.

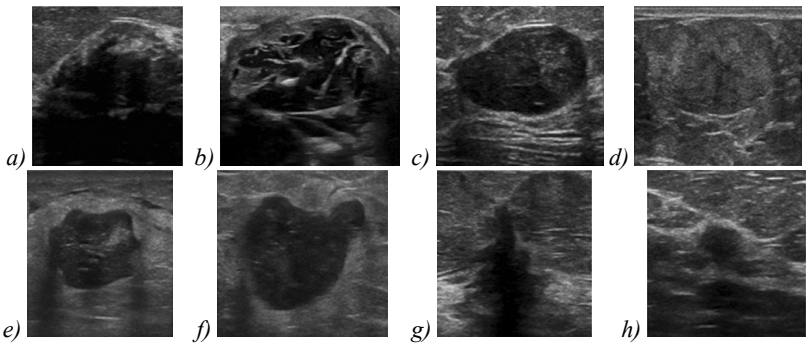

Fig. 1. The examples of benign (upper row (a - d)) and malignant (lower row (e - h)) lesions included into the analysis

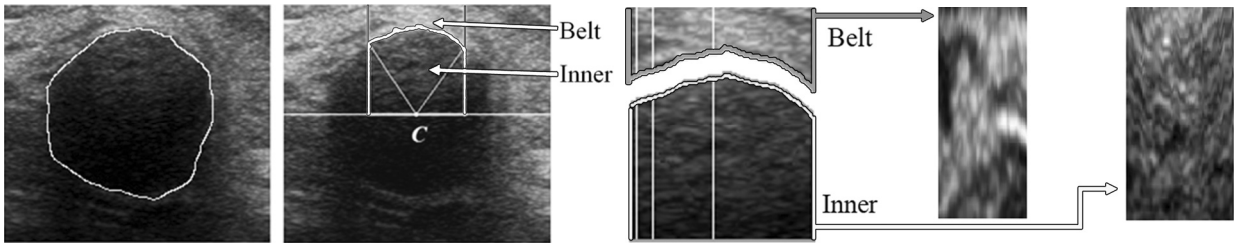

Fig. 2. (a) The source image; (b) the area bounded by the vertical lines and the horizontal line passing through the point C; (c) the separated inner and belt areas (vertical white lines correspond to the ones along which the interpolation was carried out); (d) the results of the linear interpolation of the brightness pixels of the each column for the inner (white arrow) and belt (grey arrow) regions

The VGG16 network yields 4096 features in its output for a single image, ResNet-18 provides 512 features, and Inception-ResNet generates 1536 features. Considering the assumed distinction in features between the inner and outer lesion parts, the difference between the features was also calculated. The features obtained from the three images and the difference in features between the inner and outer parts were combined into one feature vector, resulting in a total of 4 times more features than what the deep learning network yielded for a single image. So, when using the VGG16 network, the complete feature vector contained $4096 \times 4 = 16384$ features, for ResNet-18, it was 2048 features, and for Inception-ResNet, it was 6144 features.

In the implementation of the DL approach, the image pixels inside and outside the contour were processed. For each column of pixels, linear interpolation was used to ensure that the number of pixels in each vertical column became 512. This interpolation resulted in the formation of two additional rectangular images representing the inner and belt regions of the upper part of the lesion (fig. 2*d*).

Fig. 3 shows a diagram illustrating the implementation of the DL approach, with the ResNet-18 network being depicted as the DL network. Each of the three images (the entire image, images of the inner and belt parts of the lesion) was inputted into the DL network to extract image features. The networks utilized in this process were VGG-16 (generating 4096 features), ResNet-18 (generating 512 features), and InceptionResNetV2 (generating 1536 features).

Since there was an assumed difference in features between the inner and belt parts of the lesion, the difference in features for the corresponding images was also calculated. The features obtained from the three images (resulting in 1536 features) and the difference in features between the inner and belt parts of the lesion (resulting in 512 features) were combined into a single feature vector of 2048 features. This feature vector was then subjected to three significant feature selection blocks based on the ReliefF algorithms [9], FSCNCA [10], and LASSO method [11]. Feature selection methods are commonly employed when dealing with a large number of features and a relatively small sample size.

The ReliefF algorithm determines the significance of the features using the k-nearest neighbors method. Meanwhile, the FSCNCA algorithm performs feature selection for classification by utilizing the diagonal adaptation method of the environment component analysis with regularization. On the other hand, the LASSO method returns significant linear regression coefficients in the least squares method. The mathematical equation of the Lasso model [11] can be expressed as:

$$\arg\min\left(\sum_{i=1}^{n}(y_i - \sum_{j=1}^{m}\beta_j x_{ij})^2 + \lambda|\beta|\right),$$

where x_{ij} is the value of the independent variable (values of the features under consideration for 494 ultrasound images), y_i is the value of the dependent variable (–1 for benign and 1 for malignant), λ is the penalty parameter ($\lambda \geq 0$), β_j is the regression coefficient, $n = 494$, m is the number of the features.

Distinguishing features selected by these three methods were combined into one feature vector. The SVM was used to classify the obtained feature vectors. Accuracy, sensitivity, and specificity describe the performance of the classification models in terms of true positive (TP), true negative (TN), false negative (FN), and false positive (FP) results:

Accuracy $=(TN+TP)/(TN+TP+FN+FP)=$ (Number of correct assessments)/Number of all assessments).

Sensitivity $=TP/(TP+FN)=$(Number of true positive assessment)/(Number of all positive assessment).

Specificity $=TN/(TN+FP)=$(Number of true negative assessment) / (Number of all negative assessment).

Our study was conducted in three stages.

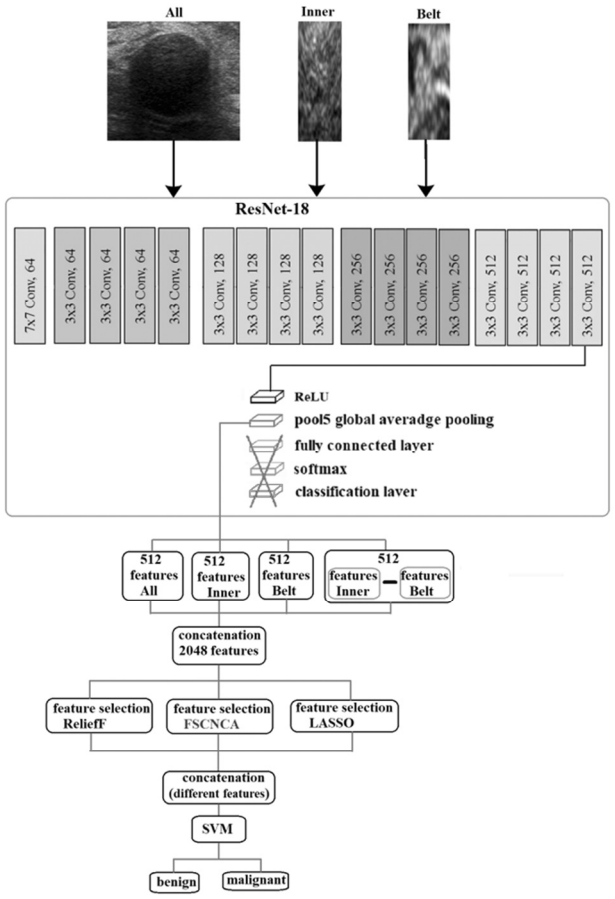

Fig. 3. Schematic diagram of the classification algorithm for breast ultrasound image

In the first stage, we evaluated the results of non-modified DL networks (VGG-16, ResNet-18, InceptionResNetV2). We used supervised transfer learning to train the networks.

Lately, the SVM method has been frequently used as a classifier in deep learning networks instead of the traditional fully connected layers (fully connected layer, softmax and classification layer) [12 – 14].

This is because it is challenging to obtain large homogeneous medical datasets – partially scanned on the same equipment with identical settings. As shown in the mentioned works [12 – 14], SVM demonstrates better classification results than fully connected layers in such conditions.

So, in the second stage, we evaluated the results of lesion classification using the SVM model.

To train the SVM, a linear kernel was used with 200 training iterations and a tolerance error of 0.000001. When assessing the classification quality of the machine learning model, k-fold cross-validation was applied.

We used the features obtained from the modified DL networks for both training and testing. To do this, we removed the last layers (fully connected layer, softmax, and classification layer) from the pre-trained networks (VGG-16, ResNet-18, InceptionResNetV2).

In the final stage, we evaluated the classification results using SVM, but we selected the obtained features from the modified DL networks based on their significance using the ReliefF, FSCNCA, and LASSO methods.

2. Results

Tab. 2 shows the results of lesion classification using different DL models, and it's worth noting that all models demonstrate similar outcomes.

Tab. 2. DL models evaluation. Note: The best index values are given in bold

Model	Accuracy	Sensitivity	Specificity
VGG-16	0.878	0.864	0.895
Resnet-18	**0.911**	**0.924**	**0.895**
InceptionResNetV2	0.902	0.923	0.879

Tab. 3 shows the results of SVM classification by employing a combination of four DL feature vectors derived from three images: the entire image (see fig. 2*a*), images of the inner and belt parts of the lesion (see fig. 2*d*), and the discrepancy in feature vector values between the inner and belt parts (without feature selection using the ReliefF, FSCNCA, and LASSO methods). The table demonstrates that assessing image features in the inner and belt regions of the lesion enhanced the classification quality.

Tab. 3. SVM model based on the different DL feature sets evaluation with no selection of the significant features. Note: The best index values are given in bold

Model	Accuracy	Sensitivity	Specificity
VGG-16	0.953	**0.966**	0.939
Resnet-18	0.939	0.952	0.924
InceptionResNetV2	**0.967**	0.955	**0.982**

Tab. 4 displays the outcomes of SVM classification utilizing four DL feature vectors derived from three images: the entire image (see fig. 2*a*), images of the inner and belt parts of the lesion (see fig. 2*d*), and the discrepancy in feature vector values between the inner and belt parts. These features were combined after selecting the significant features using three different methods (ReliefF, FSCNCA, and LASSO). The table shows the results of the classification based on this combined set of features.

Tab. 4. SVM model based on the different DL feature sets evaluation with no selection of the significant features. Note: The best index values are given in bold

Model	Accuracy	Sensitivity	Specificity
VGG-16	0.980	0.985	0.974
Resnet-18	0.974	**0.989**	0.957
InceptionResNetV2	**0.984**	0.985	**0.983**

It is evident from tab. 4 that the inclusion of significant features has enhanced the quality of classification for all models. The number of significant features selected by the analyzed methods from the various models can be observed in tab. 5.

Tab. 5. Number of features selected by different methods

Model	Feature vector	Number of features selected			
		ReliefF	FSCNCA	LASSO	Total
VGG-16	A	4	7	9	20
	XI	0	1	8	9
	XB	1	3	7	11
	XI–XB	2	7	8	17
	Total	7	18	32	57
Resnet-18	A	3	6	32	41
	XI	1	1	22	24
	XB	3	0	18	21
	XI–XB	3	8	15	26
	Total	10	15	87	112
Inception ResNetV2	A	6	5	18	29
	XI	1	1	3	5
	XB	1	0	6	7
	XI–XB	2	9	15	26
	Total	10	15	42	67

In tab. 5, *XA* represents the feature vector obtained from the selected DL model for the original image *A* (fig. 2*a*), *XI* and *XB* represent the feature vectors obtained from the selected DL model for the internal and belt parts of the image (fig. 2*d*), and *XI - XB* represents the difference vector of the corresponding feature vectors.

From tab. 5, it is apparent that the most significant features are selected from the feature vector of the original image *A* and the feature difference vector *XI – XB*.

Fig. 4 exhibits the receiver operating characteristic (ROC) curves for various classification approaches along with their corresponding area under curve (AUC) values. The red dots indicate the position of the current classifier. Fig. 4*a–c* correspond to the models and results presented in tab. 2, while Fig. 4*d-f* correspond to the ones presented in tab. 3, and Fig. 4*g-i* correspond to those in tab. 4. These figures demonstrate that the utilization of additional images enhances the classification quality. The feature selection module has also shown improvement in the classification quality for all DL models.

Moreover, the selection of significant features has led to a considerable reduction in the number of image features, enabling the construction of feature value distributions for benign and malignant breast lesions (see fig. 5, model VGG-16).

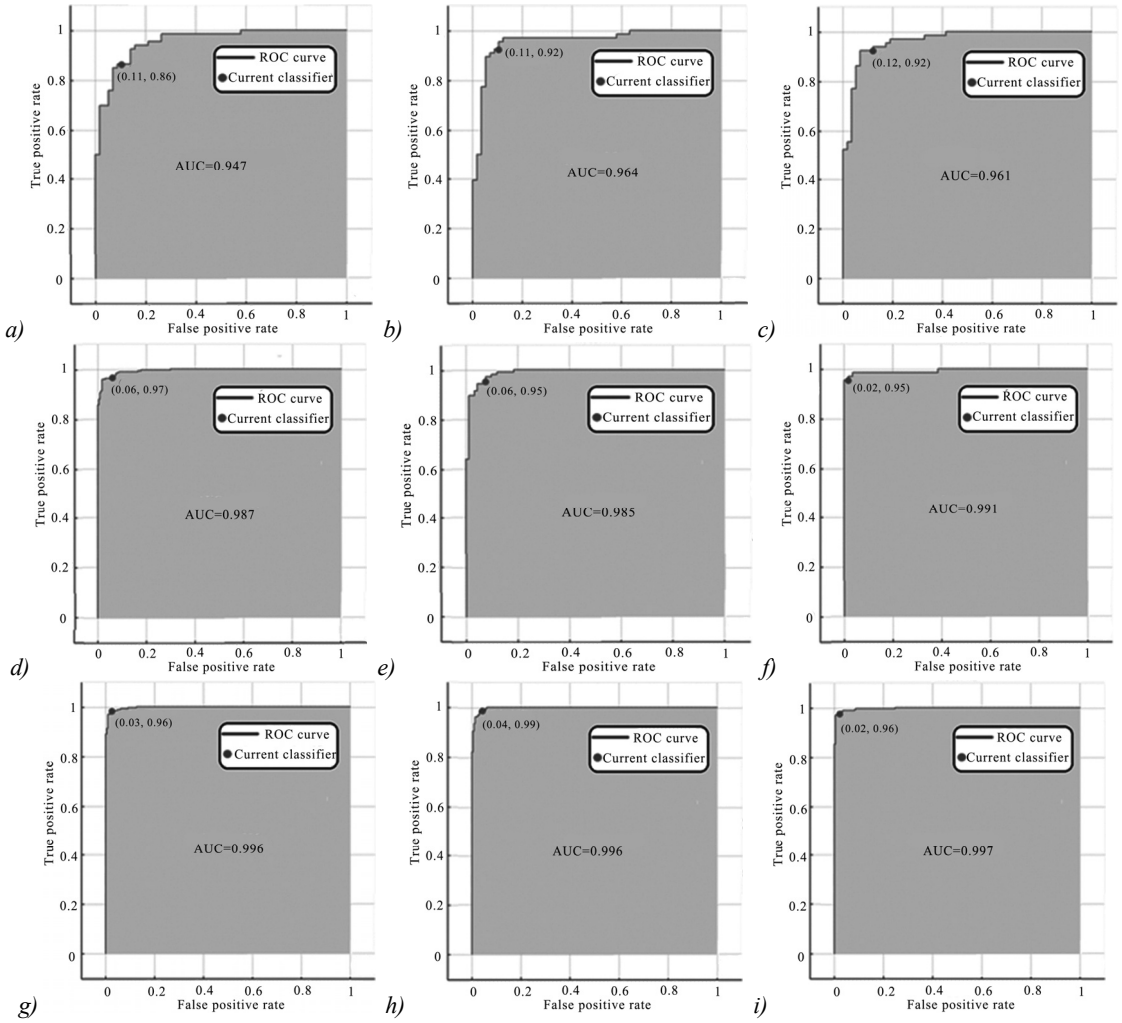

Fig. 4. ROC curves and AUC values of the classification method based on the results listed in table 2(a – c), table 3 (d – f) and table 4 (g – i)

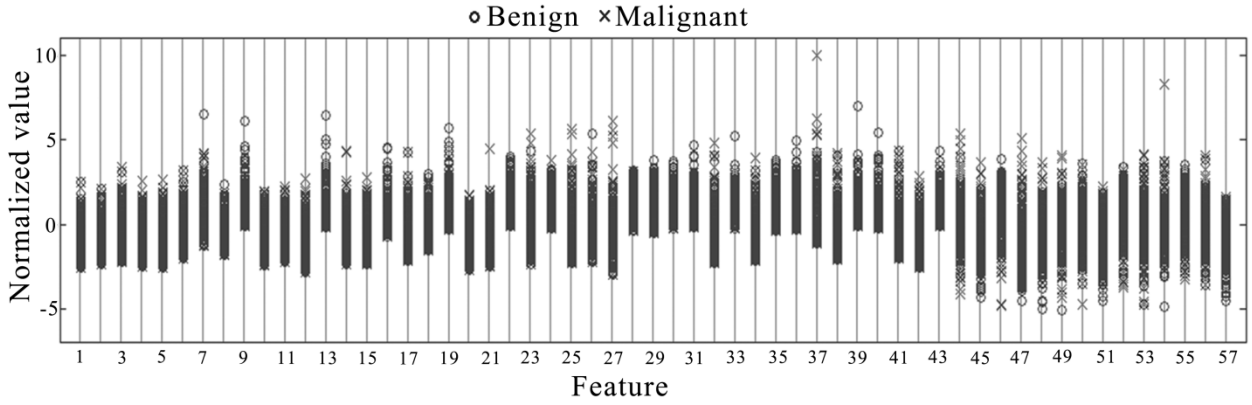

Fig. 5. Normalized distributions of all features for benign and malignant breast lesions in the VGG-16 model

3. Discussion

The presence of noise and aliasing characteristics in ultrasound (US) images poses challenges in obtaining accurate classification results using only the original image [15, 16]. As a result, there has been increasing discussion regarding image classification based on combined data from multiple images [17 – 20].

Previous attempts to discriminate between benign and malignant breast lesions on ultrasound images have focused on textural features and deep learning, but they did not selectively extract the area around the lesion or evaluate only that specific area of fixed width [21 – 25].

Furthermore, clinicians often rely on the blurring of lesion edges as an important indicator to differentiate between benign and malignant breast lesions [26]. To address this, our work proposes considering the entire lesion, including its internal and external (belt) parts, as three separate images.

Another significant aspect is the specific part of the lesion included in the processing. The upper 120° sector of the lesion is known to be relatively free from US artifacts, while the side and lower sectors contain numerous unpredictable artifacts that may potentially reduce the classification quality [27]. To enhance the classification quality, we utilized the upper lesion sector for calculations.

It is worth noting that the test set comprised images obtained from various ultrasound systems with different parameters to assess the impact on model correctness. Fig. 6 depicts ultrasound images of malignant breast lesions that were mistakenly classified as benign by the proposed method.

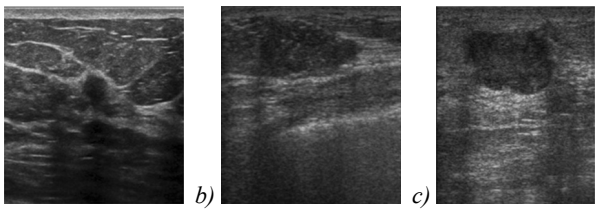

Fig. 6. Images of malignant breast lesions that were erroneously classified as benign by the proposed method

The incorrect classification of the image in fig. 6*a* may be attributed to the small proportion of training images similar in terms of acquisition parameters. This highlights the importance of standardizing acquisition parameters and ensuring proper image quality for the developed model. Additionally, fig. 6*b* presents a complex image where the lesion of interest is not clearly defined visually. Moreover, pronounced acoustic shadows in the left part of the lesion, caused by insufficiently tight contact of the ultrasound probe with the skin, and a similar problem on the right side of the lesion in fig. 6*c* further indicate the need for improved image quality and standardized acquisition parameters. It might be reasonable to include images with typical artifacts in the training set to address these issues.

Classification machine learning methods such as Support Vector Machines, Naive Bayes, Random Forest, or Logistic Regression are commonly used for breast cancer detection and classification, relying on the handcrafted feature extraction step [28, 29]. SVM, for example, is widely employed for classifying image features obtained using DL networks [30 – 34]. Although these approaches demonstrate good accuracy, they often suffer from a high false positive error rate. To mitigate this, we utilized pretrained modified DL networks for feature extraction.

Three DL models, VGG-16, ResNet-18, and InceptionResNetV2, were employed to extract features from ultrasound images. Since these DL networks were originally developed to classify 1000 different types of images, the features they generate contain irrelevant information for the task of classifying only two types of images (malignant or benign). To address this, we employed supervised transfer learning, which has proven to be effective in training DL networks for medical images [35, 36].

However, DL networks often produce a large number of features, many of which are not informative for the task. To overcome this issue, appropriate feature selection methods are implemented. For example, principal component analysis (PCA) or LASSO methods have been used to reduce redundant information in feature selection [37, 38]. In our work, we propose using multiple feature selection methods and combining the selected features for classification.

Our study results demonstrate that not only the area of the lesion (feature vector *XI*) is crucial but also the area

surrounding the lesion (feature vector *XB*). After significant feature selection, we identified nine features from feature vector *XI* and eleven features from feature vector *XB* among the features of the DL model VGG-16 (as shown in tab. 5). Similarly, for the ResNet-18 DL model, there were 24 and 21 features, and for the InceptionResNetV2 DL model, 5 and 7 features, respectively. Hence, the features of the belt area surrounding the lesion are just as important as the features of the lesion itself.

Indeed, the feature selection analysis presented in tab. 5 highlights that not only the features of the images themselves play a crucial role but also the differences in feature values for different parts of the region of interest. It is noteworthy that, for all the analyzed DL models, the number of selected significant features for the difference of feature values $XI-XB$ is greater than the number of features selected from the *XB* or *XI* feature vectors alone.

As depicted in table 5 and fig. 4$g-i$, the inclusion of a feature selection block utilizing multiple algorithms with different principles of feature selection significantly enhances the classification quality when employing transfer learning techniques. This demonstrates the importance of considering the discrepancy in feature values between the lesion and its surrounding area for improved classification performance.

In general, for the classification of medical images, specific datasets that are not publicly accessible are used, such as the data from the Department of Ultrasound of the First Hospital of Quanzhou City, Fujian Province, China [37], obtained with Philips IU22 and Philips IU Elite machines, or combined datasets from multiple public and/or non-public sources, such as in [26], due to their limited quantity in a single dataset.

However, each dataset often specific for the equipment on which the ultrasound data acquisition was performed, as data obtained using the different equipment may differ in terms of image characteristics (resolution, contrast etc.), or preprocessing might have been applied, requiring standardization during the model training. Otherwise, the question of the generalization ability of the trained model arises.

In public databases, image resolution is often reduced to decrease the size of the database, for example [39]. Models trained on these data cannot be used in clinical practice due to the discrepancy in image resolution between the database and the images obtained from modern ultrasound machines.

Using the model provided by the authors for other classification tasks with different types of data is possible, but it requires a new selection of hyperparameters for the model itself (such as the number of selected features, the number of classes, etc.), labeling a new dataset, and retraining or fine-tuning the entire network.

Conclusions

Our results show that the SVM, in conjunction with methods for significant feature selection (ReliefF, FSCNCA, and LASSO), improves the quality of breast lesion classification in ultrasound images. The proposed algorithm achieved sufficient accuracy in solving the clinical task.

References

[1] Bray F, Ferlay J, Soerjomataram I, Siegel RL, Torre LA, Jemal A. Global cancer statistics 2018: GLOBOCAN estimates of incidence and mortality worldwide for 36 cancers in 185 countries. Cancer J Clin 2018; 68: 394-424. DOI: 10.3322/caac.21492.

[2] Seely JM, Alhassan T. Screening for breast cancer in 2018 – what should we be doing today? Curr Oncol 2018; 25(1): S115-S124. DOI: /10.3747/co.25.3770.

[3] Lauby-Secretan B, Scoccianti C, Loomis D, Benbrahim-Tallaa L, Bouvard V, Bianchini F, Straif K. Breast-cancer screening – viewpoint of the IARC Working Group. N Engl J Med 2015; 372(24): 2353-2358. DOI: 10.1056/NEJMsr1504363.

[4] Thigpen D, Kappler A, Brem R. The role of ultrasound in screening dense breasts – a review of the literature and practical solutions for implementation. Diagnostics (Basel) 2018; 8(1): 1-20. DOI: 10.3390/diagnostics8010020.

[5] Berg WA, Blume JD, Cormack JB, Mendelson EB, Lehrer D, Bohm-Velez M, Pisano ED, Jong RA, Evans WP, Morton MJ, Mahoney MC, Larsen LH, Barr RG, Farria DM, Marques HS, Boparai K. Combined screening with ultrasound and mammography vs mammography alone in women at elevated risk of breast cancer. JAMA 2008; 299(18): 2151-2163. DOI: 10.1001/jama.299.18.2151.

[6] Corsetti V, Houssami N, Ferrari A, Ghirardi M, Bellarosa S, Angelini O, Bani C, Sardo P, Remida G, Galligioni E, Ciatto S. Breast screening with ultrasound in women with mammography-negative dense breasts: evidence on incremental cancer detection and false positives, and associated cost. Eur J Cancer 2008; 44(4): 539-544. DOI: 10.1016/j.ejca.2008.01.009.

[7] Egoshin IA, Pasynkov DV, Kolchev AA, Kliouchkin IV, Pasynkova OO. Segmentation of breast focal lesions on the ultrasound image. Biomed Eng 2020; 54: 99-103. DOI: 10.1007/s10527-020-09982-6.

[8] Deng J, Dong W, Socher R, Li L-J, Li K, Fei-Fei L. ImageNet: A large-scale hierarchical image database. 2009 IEEE Conf on Computer Vision and Pattern Recognition 2009: 248-255. DOI: 10.1109/CVPR.2009.5206848.

[9] Robnik-Sikonja M, Kononenko I. Theoretical and empirical analysis of ReliefF and RReliefF. Machine Learn 2003; 53: 23-69. DOI: 10.1023/A:1025667309714.

[10] Yang W, Wang K, Zuo W. Neighborhood component feature selection for high-dimensional data. J Comput 2012; 7(1): 161-168. DOI: 10.4304/jcp.7.1.161-168.

[11] Muthukrishnan R, Rohini R. LASSO: A feature selection technique in predictive modeling for machine learning. 2016 IEEE Int Conf on Advances in Computer Applications (ICACA) 2016: 18-20. DOI: 10.1109/ICACA.2016.7887916.

[12] Alzubaidi L, Fadhel MA, Al-Shamma O, Zhang J, Duan Y. Deep learning models for classification of red blood cells in microscopy images to aid in sickle cell anemia diagnosis. Electronics 2020; 9: 427. DOI: 10.3390/electronics9030427.

[13] Zahoor MM, Qureshi SA, Bibi S, Khan SH, Khan A, Ghafoor U, Bhutta MR. A new deep hybrid boosted and ensemble learning-based brain tumor analysis using MRI. Sensors (Basel) 2022; 22(7): 2726. DOI: 10.3390/s22072726.

[14] Tan S, Pan J, Zhang J, Liu Y. CASVM: An efficient deep learning image classification method combined with SVM. Appl Sci 2022; 12(22): 11690. DOI: 10.3390/app122211690.
[15] Virmani J, Agarwal R. Deep feature extraction and classification of breast ultrasound images. Multimed Tools Appl 2020; 79(37): 27257-27292. DOI: 10.1007/s11042-020-09337-z.
[16] Drukker K, Giger ML, Vyborny CJ, Mendelson EB. Computerized detection and classification of cancer on breast ultrasound. Acad Radiol 2004; 11(5): 526-535. DOI: 10.1016/S1076-6332(03)00723-2.
[17] Shakya A, Biswas M, Pal M. CNN-based fusion and classification of SAR and optical data. Int J Remote Sens 2020; 41(22): 8839-8861. DOI: 10.1080/01431161.2020.1783713.
[18] Tan C, Sun Y, Li G, Jiang G, Chen D, Liu H. Research on gesture recognition of smart data fusion features in the IoT. Neural Comput Appl 2019; 32(22): 16917-16929. DOI: 10.1007/s00521-019-04023-0.
[19] Dong H, Song K, He Y, Xu J, Yan Y, Meng Q. PGA-Net: Pyramid feature fusion and global context attention network for automated surface defect detection. IEEE Trans Ind Inform 2019; 16(12): 7448-7458. DOI: 10.1109/TII.2019.2958826.
[20] Ioffe S, Szegedy C. Batch normalization: Accelerating deep network training by reducing internal covariate shift. Proc 32nd Int Conf on Machine Learning 2015; 37: 448-456.
[21] Klimonda Z, Karwat P, Dobruch-Sobczak K, Piotrzkowska-Wroblewska H, Litniewski J. Breast-lesions characterization using Quantitative Ultrasound features of peritumoral tissue. Sci Rep 2019; 9: 7963. DOI: 10.1038/s41598-019-44376-z.
[22] Bahareh B, Hamze R, Tehrani Ali KZ, Hassan R. Deep classification of breast cancer in ultrasound images: more classes, better results with multi-task learning. Proc SPIE 2021; 11602: 116020S. DOI: 10.1117/12.2581930.
[23] Nemat H, Fehri H, Ahmadinejad N, Frangi AF, Gooya A. Classification of breast lesions in ultrasonography using sparse logistic regression and morphology-based texture features. Med Phys 2018; 45(9): 4112-4124. DOI: 10.1002/mp.13082.
[24] Jabeen K, Khan MA, Alhaisoni M, Tariq U, Zhang Y-D, Hamza A, Mickus A, Damasevicius R. Breast cancer classification from ultrasound images using probability-based optimal deep learning feature fusion. Sensors 2022; 22(3): 807. DOI: 10.3390/s22030807.
[25] Badawy SM, Mohamed AE-NA, Hefnawy AA, Zidan HE, GadAllah MT, El-Banby GM. Automatic semantic segmentation of breast tumors in ultrasound images based on combining fuzzy logic and deep learning – A feasibility study. PLoS ONE 2021; 16(5): e0251899. DOI: 10.1371/journal.pone.0251899.
[26] Zhuang Z, Yang Z, Joseph Raj AN, Wei C, Jin P, Zhuang S. Breast ultrasound tumor image classification using image decomposition and fusion based on adaptive multi-model spatial feature fusion. Comput Methods Programs Biomed 2021; 208: 106221. DOI: 10.1016/j.cmpb.2021.106221.
[27] Zhou Z, Wu S, Chang KJ, Chen WR, Chen YS, Kuo WH, Lin CC, Tsui PH. Classification of benign and malignant breast tumors in ultrasound images with posterior acoustic shadowing using half-contour features. J Med Biol Eng 2015; 35(2): 178-187. DOI: 10.1007/s40846-015-0031-x.
[28] Yassin NI, Omran S, El Houby EM, Allam H. Machine learning techniques for breast cancer computer aided diagnosis using different image modalities: a systematic review. Comput Methods Programs Biomed 2018; 156: 25-45. DOI: 10.1016/j.cmpb.2017.12.012.-13.
[29] Naji MA, Filali SE, Aarika K, Benlahmar EH, Abdelouhahid RA, Debauche O. Machine learning algorithms for breast cancer prediction and diagnosis. Procedia Comput Sci 2021; 191: 487-492. DOI: 10.1016/j.procs.2021.07.062.
[30] Kim S, Kavuri S, Lee M. Deep network with support vector machines. In: Lee M, Hirose A, Hou ZG, Kil RM, eds. Neural information processing. Berlin, Heidelberg: Springer-Verlag; 2013: 458–465. DOI: 10.1007/978-3-642-42054-2_57.
[31] Jafarpisheh N, Teshnehlab M. Cancers classification based on deep neural networks and emotional learning approach. IET Syst Biol 2018; 12: 258-263. DOI: 10.1049/iet-syb.2018.5002.
[32] Vogado LH, Veras RM, Araujo FH, Silva RR, Aires KR. Leukemia diagnosis in blood slides using transfer learning in CNNs and SVM for classification. Eng Appl Artif Intell 2018; 72: 415-422. DOI: 10.1016/j.engappai.2018.04.024.
[33] Nanni L, Ghidoni S, Brahnam S. Deep features for training support vector machines. J Imaging 2021; 7(9): 117. DOI: 10.3390/jimaging7090177.
[34] Khan MA, Javed MY, Sharif M, Saba T, Rehman A. Multi-model deep neural network based features extraction and optimal selection approach for skin lesion classification. 2019 Int Conf on Computer and Information Sciences (ICCIS) 2019: 1-7. DOI: 10.1109/ICCISci.2019.8716400.
[35] Al-masni M, Al-antari MA, Park J-M, Gi G, Kim T-Y, Rivera P, Valarezo AE, Choi M-T, Han S-M, Kim T-S. Simultaneous detection and classification of breast masses in digital mammograms via a deep learning YOLO-based CAD system. Comput Methods Programs Biomed 2018; 157: 85-94. DOI: 10.1016/j.cmpb.2018.01.017.
[36] Jiang F, Liu H, Yu S, Xie Y. Breast mass lesion classification in mammograms by transfer learning. Proc 5th Int Conf on Bioinformatics and Computational Biology (ICBCB) 2017: 59-62. DOI: 10.1145/3035012.3035022.
[37] Liu W, Liu P, Wu X, Du Y. Breast tumor ultrasound image classification method based on the fusion of deep network features and texture morphological features. Int Conf on Public Health and Data Science (ICPHDS) 2021: 81-85. DOI: 10.1109/ICPHDS53608.2021.00025.
[38] Kolchev AA, Pasynkov DV, Egoshin IA, Kliouchkin IV, Pasynkova OO. Cystic (including atypical) and solid breast lesion classification using the different features of quantitative ultrasound parametric images. Int J CARS 2022; 17: 219-228. DOI: 10.1007/s11548-021-02522-x.
[39] Al-Dhabyani W, Gomaa M, Khaled H, Fahmy A. Dataset of breast ultrasound images. Data in Brief 2020; 28: 104863. DOI: 10.1016/j.dib.2019.104863.

Authors' information

Alexey Anatolevich Kolchev (b. 1965) Dr, PhD, associate professor in Kazan (Volga region) Federal University, Ministry of Education and Science of Russian Federation. Research interests: mathematical modeling, digital signal and image processing, deep learning, machine learning. E-mail: kolchevaa@mail.ru ORCID: 0000-0002-1692-2558.

Dmitry Valerevich Pasynkov (b. 1975) MD, PhD, associate professor, head of Radiology and Oncology department in Mari State University, Ministry of Education and Science of Russian Federation, assistant professor of Ultrasound Diagnostics department in Kazan State Medical Academy - Branch Campus of the Federal State Budgetary Educational Institution of Further Professional Education «Russian Medical Academy of Continuous Professional Education», Ministry of Healthcare of the Russian Federation. Research interests: radiology in oncology, radiological image analysis. E-mail: *passynkov@mail.ru* ORCID: 0000-0003-1888-2307.

Ivan Aleksandrovich Egoshin (b. 1991) junior researcher at Mari State University, Ministry of Education and Science of Russian Federation. Research interests: digital signal and image processing, radiomics, artificial intelligence, machine learning, programming. E-mail: *jungl91@mail.ru* ORCID: 0000-0003-0717-0734.

Ivan Vladimirovich Kliouchkin (b. 1948) MD, DSc, Professor of General Surgery department in Kazan Medical University, Ministry of Health of Russian Federation. Research interests: radiology, medical image analysis.
E-mail: *hirurgivan@rambler.ru* ORCID: 0000-0001-5052-2921.

Olga Olegovna Pasynkova (b. 1977) MD, PhD, associate professor of Fundamental Medicine department in Mari State University, Ministry of Education and Science of Russian Federation. Research interests: fundamental and clinical medicine, ultrasound diagnostics, mathematical modeling.
E-mail: *olgaved@inbox.ru* ORCID: 0000-0001-9117-8151.

Received September 13, 2023. The final version – December 26, 2023.